Direct Simulation of the Surface Manifestation of Internal Gravity Waves with a Wave-Current Interaction Model

Liangyi Yue,[a] Xuanting Hao,[b] Lian Shen,[b] Oliver B. Fringer,[a]

[a] *The Bob and Norma Street Environmental Fluid Mechanics Laboratory, Department of Civil and Environmental Engineering, Stanford University, Stanford, California*

[b] *The St. Anthony Falls Laboratory and Department of Mechanical Engineering, University of Minnesota, Minneapolis, Minnesota*

Corresponding author: Liangyi Yue, liangyi@stanford.edu

Early Online Release: This preliminary version has been accepted for publication in *Journal of Physical Oceanography*, may be fully cited, and has been assigned DOI 10.1175/JPO-D-22-0097.1. The final typeset copyedited article will replace the EOR at the above DOI when it is published.

ABSTRACT: Internal solitary waves in the ocean are characterized by the surface roughness signature of smooth and rough bands that are observable in synthetic aperture radar satellite imagery, which is caused by the interaction between surface gravity waves and internal wave-induced surface currents. In this work, we study the surface signature of an internal wave packet in deep water over a large range of spatial scales using an improved wave-current interaction model that supports a moving surface current corresponding to a propagating internal gravity wave. After validating the model by comparison to previously published numerical results in Hao and Shen (2020), we investigate a realistic case based on a recent comprehensive field campaign conducted by Lenain and Pizzo (2021). Distinct surface manifestation caused by internal waves can be directly observed from the surface waves and the associated surface wave steepness. Consistent with observations, the surface is relatively rough where the internal wave-induced surface current is convergent ($\partial U/\partial x < 0$), while it is relatively smooth where the surface current is divergent ($\partial U/\partial x > 0$). The spatial modulation of the surface wave spectrum is rapid as a function of along-propagation distance, showing a remarkable redistribution of energy under the influence of the propagating internal wave packet. The directional wavenumber spectra computed in the smooth and rough regions show that the directional properties of the surface wave spectra are also rapidly modulated through strong wave-current interactions. Good agreement is found between the model results and the field observations, demonstrating the robustness of the present model in studying the impact of internal waves on surface gravity waves.

Accepted for publication in *Journal of Physical Oceanography*. DOI 10.1175/JPO-D-22-0097.1.

SIGNIFICANCE STATEMENT: The purpose of this study is to better understand the physical processes leading to the bands of rough and smooth surface waves arising from internal gravity waves. The surface manifestation of internal gravity waves allows them to be measured remotely via surface imagery which can provide insight into their nonlinear behavior and sources and fate, which can ultimately inform the local stratification for assimilation into larger-scale models. Our results highlight the application of wave-current interaction models to the study of the interaction of surface waves with internal gravity waves and indicate strong modulation of the surface wave spectra over relatively short time scales despite the long time scales associated with the internal wave propagation.

1. Introduction

Internal waves are a common feature of coastal and open-ocean waters. As a train of internal waves propagates, it leaves on the ocean surface a distinct signature of alternating rough and smooth regions of increased and decreased surface wave steepness. The surface roughness induces a variation in the strength of radar backscatter signals, such that the signature of internal waves appears in the form of bright and dark bands when observed using satellite radar imaging (e.g. Bai et al. 2014; Magalhães and da Silva 2018; Magalhães et al. 2021; Santos-Ferreira et al. 2022). The surface signature obtained via remote sensing thus enables identification of internal waves over large regions of the ocean (Helfrich and Melville 2006), particularly internal solitary-like waves with wave lengths of the order of hundreds of meters. Relative to the background flow, the associated surface roughness due to nonlinear internal waves causes wind velocity and stress variance in the marine atmospheric surface layer (Ortiz-Suslow et al. 2019). In spite of its importance, it remains a challenge to investigate the impact of internal waves on ocean surface waves due to a lack of effective and accurate quantitative observations of the surface gravity wave field modified by internal waves.

The fully nonlinear interaction of internal waves and a free surface wave occurs over a broad range of time and length scales associated with a variety of different forcing mechanisms (Craig et al. 2012). Consequently, the ability to study this process with traditional observational techniques (e.g., moored water-column measurements or research vessels) is limited due to access and/or cost. Moreover, considering the fast time scale of surface gravity waves relative to the time scales

Accepted for publication in *Journal of Physical Oceanography*. DOI 10.1175/JPO-D-22-0097.1.

of satellite coverage, the role of satellite remote sensing is limited. Therefore, airborne remote sensing is a promising technique to directly measure the short surface waves. A comprehensive field campaign was conducted by Lenain and Pizzo (2021) off the coast of Point Sal, California, in September 2017 to study the interaction between surface and internal waves. Using a unique combination of airborne remote sensing observations along with in situ surface and subsurface measurements, they quantified the rapid modification of the spectral properties of surface waves over short spatial scales (100 m or less) in internal wave packets and found that the surface waves are significantly modulated by the surface currents induced by the waves.

Most theoretical studies address the question of the surface signature of an internal wave through wave-current interaction models, assuming that the surface manifestation is indirectly caused by the action of a specified current induced by the internal wave. These models are generally based on ray-tracing theories similar to geometrical optics and widely used in applications to remote sensing of internal waves, incorporating phase-averaged models based on either a wave energy balance equation incorporating radiation stresses (e.g. Lewis et al. (1974)), or a wave action balance equation combined with ray theory (e.g. Bakhanov and Ostrovsky (2002)). However, these theories have several shortcomings depending on the situation under consideration. First, phase-averaged theories may lead to singularities because they do not account for bound and reflected surface waves (Smith 1983, see also the discussions in Hao and Shen 2020), which are important for complex surface signature formation. Second, there is currently no way to model the source terms for wave-wave interactions, wave energy input (wind input) or dissipation (wave breaking). Third, the relaxation assumption (Hughes 1978; Lyzenga and Bennett 1988) that the current-modulated spectrum only deviates a small amount from the unmodulated spectrum may not hold for strong nonlinear interactions like those observed by Lenain and Pizzo (2021).

Some of these shortcomings were addressed in two-layer ocean models in which the internal and surface waves could have substantially different length scales. Craig et al. (2012) studied the resonant interaction of nonlinear internal waves with the surface modes by coupling a Korteweg–de Vries (KdV) equation and a Schrödinger equation, finding that the surface signature is generated by a process analogous to radiative absorption. Similarly, Jiang et al. (2019) investigated the generation of surface waves at the leading edge of an internal wave and the asymmetric behaviour of long surface waves with a Boussinesq-type, two-layer model. Using explicit, second-order

Accepted for publication in *Journal of Physical Oceanography*. DOI 10.1175/JPO-D-22-0097.1.

nonlinear evolution equations in Hamiltonian form in a two-layer system, Taklo and Choi (2020) focused on the surface wave modulation by the group resonance mechanism that corresponds to near-resonant triad interactions between a long internal wave and short surface waves. To study the nonlinear interaction between two-dimensional surface and internal waves, a spectral model was derived by Choi et al. (2021) from an explicit Hamiltonian for a two-layer system after decomposing the surface and interface motions into the two wave modes through a canonical transformation. But, in deriving model equations for the case of resonant internal and surface mode interactions, they assumed that both the surface and internal wave fields were weakly nonlinear and that the surface wave field was narrow-banded. Therefore, it would be desirable to directly resolve a wide range of weakly nonlinear wave motions from first principles such that the impact of internal waves on the surface waves can be accurately described and modelled. Recently, Hao and Shen (2020) presented the first-ever effort to directly capture the surface roughness signature by numerically solving a deterministic wave-phase-resolved two-layer model. The wave dynamics of over four million independent components were resolved, covering the wide range of length scales between the internal wave and short surface waves. The drawbacks of simplified theories were avoided, and they found that the formation of the surface wave signature is essentially an energy-conservative process. The two-layer model was simplified by Hao et al. (2022) where the bottom boundary conditions for the upper layer were computed from an internal wave solver, providing a computationally efficient tool for simulating complex surface wave fields in the presence of large amplitude internal waves.

In the present work, we follow the method of Hao and Shen (2020) but investigate the modification of a surface wave field in deep water due to a specified internal wave-induced surface current. Compared to Hao and Shen (2020), our wave-current interaction model is more computationally efficient because only one set of model equations in Zakharov-form is solved. In addition, the initialization of our model framework is straightforward because there is no need to construct the surface elevation and velocity potential with a superposition of the eigenfunctions of the linearized two-layer system. A wave-current interaction model similar to ours has been presented by a number of studies, although the surface current is assumed to be stationary (Wu 2004; Wang et al. 2018; Pan 2020; Ducrozet et al. 2021). The present work considers a propagating surface current such that the corresponding correction is made in the wave-current interaction terms, and an efficient

Accepted for publication in *Journal of Physical Oceanography*. DOI 10.1175/JPO-D-22-0097.1.

high-order spectral (HOS) method is used to solve the model equations (Klahn et al. 2020). In addition to the distinct features of the numerical model, this study is unique because, as far as we are aware, it is the first direct simulation of the interaction of a random surface wave field with internal waves in which the results are compared to observations in a real, field-scale setting.

The remainder of this paper is organized as follows. In Section 2, we introduce the mathematical model and the experiment setup. In Section 3, we present an analysis of the surface signature induced by an internal wave packet. Finally, discussion and conclusions are given in Section 4.

2. Methodology

a. Model Formulation

The model equations for the nonlinear evolution of surface waves in the presence of a propagating irrotational surface current are presented in this section. Based on the method of variable decomposition (Pan 2020), the total free surface elevation $\eta(x,y,t)$ and velocity potential $\phi(x,y,z,t)$ are decomposed into two parts as

$$\eta = \tilde{\eta} + \bar{\eta}, \quad \phi = \tilde{\phi} + \bar{\phi}, \tag{1}$$

where $\tilde{}$ and $\bar{}$ denote the components caused by the irrotational motion of surface wave and surface current, respectively. From the fully nonlinear kinematic and dynamic boundary conditions, the model equations in Zakharov form (Zakharov 1968) involving only variables on the water surface $z = \eta$ read

$$\tilde{\eta}_t + \nabla\tilde{\eta}\cdot\nabla\tilde{\Phi} - (1+\nabla\tilde{\eta}\cdot\nabla\tilde{\eta})\,\tilde{\phi}_z + F_k = 0, \tag{2}$$

$$\tilde{\Phi}_t + g\tilde{\eta} + \frac{1}{2}\left[\nabla\tilde{\Phi}\cdot\nabla\tilde{\Phi} - (1+\nabla\tilde{\eta}\cdot\nabla\tilde{\eta})\,\tilde{\phi}_z^2\right] + F_d = 0, \tag{3}$$

where the subscripts t or z denote partial derivatives, $\nabla = (\partial/\partial x, \partial/\partial y)$ is the horizontal gradient operator, $\tilde{\Phi} = \tilde{\phi}(x,y,z=\eta,t)$ is the velocity potential induced by waves at the free surface, and g is the gravitational acceleration. Based on a Taylor series expansion and following Pan (2020), a full derivation of the above model equations is presented in Appendix A with the nonlinear surface

Accepted for publication in *Journal of Physical Oceanography*. DOI 10.1175/JPO-D-22-0097.1.

wave-current interaction terms given by

$$F_k = \nabla\tilde{\eta}\cdot\mathbf{U}|_{z=\bar{\eta}} - \tilde{\eta}\,W_z|_{z=\bar{\eta}} + \nabla\bar{\eta}\cdot\nabla\tilde{\Phi} - (2\nabla\bar{\eta}\cdot\nabla\tilde{\eta} + \nabla\bar{\eta}\cdot\nabla\bar{\eta})\,\tilde{\phi}_z, \tag{4}$$

$$F_d = \nabla\tilde{\Phi}\cdot\mathbf{U}|_{z=\bar{\eta}} - \left(\nabla\bar{\eta}\cdot\nabla\tilde{\eta} + \frac{1}{2}\nabla\bar{\eta}\cdot\nabla\bar{\eta}\right)\tilde{\phi}_z^2 + \tilde{\eta}\,(W_t + WW_z)|_{z=\bar{\eta}} + \frac{1}{2}\tilde{\eta}^2\left(W_{zt} + W_z^2\right)\Big|_{z=\bar{\eta}}. \tag{5}$$

Here, $\nabla\bar{\phi} = \mathbf{U}$ and $\bar{\phi}_z = W$ are the components of the time-dependent current at the water surface. Compared to Ducrozet et al. (2021) where the surface current is assumed to be time-invariant, correction for a moving current in F_d is represented by the terms containing time derivatives.

By prescribing the horizontal velocity at the surface due to a propagating internal wave $\mathbf{U}(x, y, z = \bar{\eta}, t)$, the interaction terms F_k and F_d expressed in Equations (4) and (5) can be computed following the description in Appendix A after specifying the corresponding current-induced surface elevation $\bar{\eta}(x, y, t)$ and vertical velocity $W(x, y, z = \bar{\eta}, t)$. In the context of potential flow, the model Equations (2) and (3) are solved using the HOS method (Dommermuth and Yue 1987) for the wave motion $\tilde{\eta}$ and $\tilde{\Phi}$ from which the total surface elevation and velocity can be computed. The present wave-current interaction model is validated in Appendix B following Hao and Shen (2020), where a phase-resolved, two-layer fluid model is used by coupling with the open-source Dubreil-Jacotin-Long (DJL) equation solver DJLES (Dunphy et al. 2011) for the internal wave-induced surface current. Contributing to the surface signature formation, asymmetric behaviour of right-moving and left-moving surface waves is found in the smooth and rough bands from the wavenumber–frequency slope spectrum calculated in the frame moving with the internal wave. This finding is similar to the conclusion drawn by Hao and Shen (2020), indicating that the present wave-current interaction model is capable of simulating the surface signature of internal waves.

b. Numerical Experiment

We study the manifestation of surface gravity waves in response to a specified current, mimicking the modulation caused by a traveling internal wave. Following the in situ measurements reported by Lenain and Pizzo (2021), the detailed setup of our numerical model is presented in this section.

Accepted for publication in *Journal of Physical Oceanography*. DOI 10.1175/JPO-D-22-0097.1.

1) Initial random directional wave field

Based on the field observations, the surface wave spectrum consists of wind-generated sea and a swell. We initialize these two components separately with irregular wave fields. For the component of wind-generated waves, we generate a modeled spectrum E_w by directly interpolating the measured background directional spectrum (figure 9(a) in Lenain and Pizzo (2021)) for high wave modes with a cut-off wavenumber of $k_c = 0.6$ rad m^{-1}. For the component of swell in the range $k < k_c$, we use the directional Pierson-Moskowitz spectrum (Pierson and Moskowitz 1964)

$$E_s(\omega,\theta) = \frac{\alpha g^2}{\omega^5}\exp\left[-\beta\left(\frac{\omega}{\omega_0}\right)^{-4}\right]D(\omega,\theta), \tag{6}$$

where $\alpha = 0.0081$ is the Phillips constant, $\beta = 0.74$, $\omega_0 = g/U_{19}$ is the spectral maximum, and U_{19} is the wind speed at a height of 19.5 m above the sea surface. In Equation (6), we implement the Mitsuyasu-type spreading function (Goda 1999)

$$D(\omega,\theta) = \begin{cases} \dfrac{2^{2r-1}}{\pi}\dfrac{\Gamma^2(r+1)}{\Gamma(2r+1)}\cos^{2r}\left(\dfrac{\theta}{2}\right) & \text{for } |\theta| \le \pi/2, \\ 0 & \text{otherwise,} \end{cases} \tag{7}$$

where Γ denotes the gamma function and the spreading parameter r depends on the frequency (Mitsuyasu et al. 1975) as

$$r = \begin{cases} r_{\max}\left(\omega/\omega_p\right)^5 & \text{for } \omega \le \omega_p, \\ r_{\max}\left(\omega/\omega_p\right)^{-2.5} & \text{for } \omega > \omega_p. \end{cases} \tag{8}$$

For engineering applications, Goda (1975) proposed to use fixed values of the spreading parameter $r_{\max}$ in Equation (8) for wind waves and swell. We take $r_{\max} = 25$ by assuming that the swell has a short decay distance, and we assume $U_{19} = 7.93$ m s^{-1} corresponding to a peak wavenumber of 0.12 rad m^{-1}. In the end, the total directional surface wave spectrum is given by a superposition of these two components as $E(\omega,\theta) = E_w + E_s$.

Similar to the measured background spectrum (Fig. 1(c)), the modeled directional wave spectrum shown in Fig. 1(a) has two peaks corresponding to swell and wind-generated waves. The peak

Accepted for publication in *Journal of Physical Oceanography*. DOI 10.1175/JPO-D-22-0097.1.

wavenumber of the wind-generated waves is around $k_p = 1$ rad m^{-1} (corresponding to a peak wavelength $\lambda_p = 6.3$ m) which relates to the peak frequency ω_p through the linear dispersion relation for waves in deep water, $\omega^2 = gk$. Following the two-step procedure outlined by Tanaka (2001), an initial ocean surface wave field for the present model can be generated from the given spectrum $E(\omega, \theta)$, and is illustrated in Fig. 1(b). The omnidirectional wave frequency spectrum, defined as the azimuthally integrated directional spectrum, is given by

$$\Psi(k) = \int_0^{2\pi} E(k, \theta) k \mathrm{d}\theta. \tag{9}$$

From the comparison of the modeled and measured spectra shown in Fig. 1(d), we find a good agreement in the high wavenumber range for $k > 0.2$ rad m^{-1} but with a noticeable difference in the low wavenumbers. According to Lenain and Pizzo (2021), wave-current interactions occur for high wavenumbers greater than roughly $k = 0.6$ rad m^{-1} such that the difference is acceptable for the purposes of our study.

2) Internal wave-induced surface current

According to Appendix A, the present model requires the horizontal surface current. Although accurate moored and remote sensing observations are reported in Lenain and Pizzo (2021), the information of $\mathbf{U}(x, y, z = \bar{\eta}, t)$ cannot be obtained directly. For example, figure 4(b) in Lenain and Pizzo (2021) shows the measured current velocity but the near surface velocity is absent. Indeed, the difficulty in obtaining a precise description of the surface current that is induced by the passage of an internal solitary wave is well known (Craig et al. 2012; Romero et al. 2017).

To model the internal wave-driven current due to the train of internal solitary waves observed by Lenain and Pizzo (2021), we construct a surface current $U(x, y, z = \bar{\eta}, t = 0)$ traveling in the x-direction using the generalized normal distribution

$$u(x) = \frac{a_u s_u}{2 l_u \Gamma(1/s_u)} \exp\left[-\left(\frac{|x - x_u|}{l_u} \right)^{s_u} \right], \tag{10}$$

where $a_u = 14.25$ m^2 s^{-1}, $l_u = 40$ m, $s_u = 2.4$, and x_u are the amplitude, scale, shape, and location parameters, respectively. By choosing the appropriate values of x_u and combining multiple $u(x)$ with alternating signs, the surface current with three peaks is generated and shown in Fig. 2(a)

Accepted for publication in *Journal of Physical Oceanography*. DOI 10.1175/JPO-D-22-0097.1.

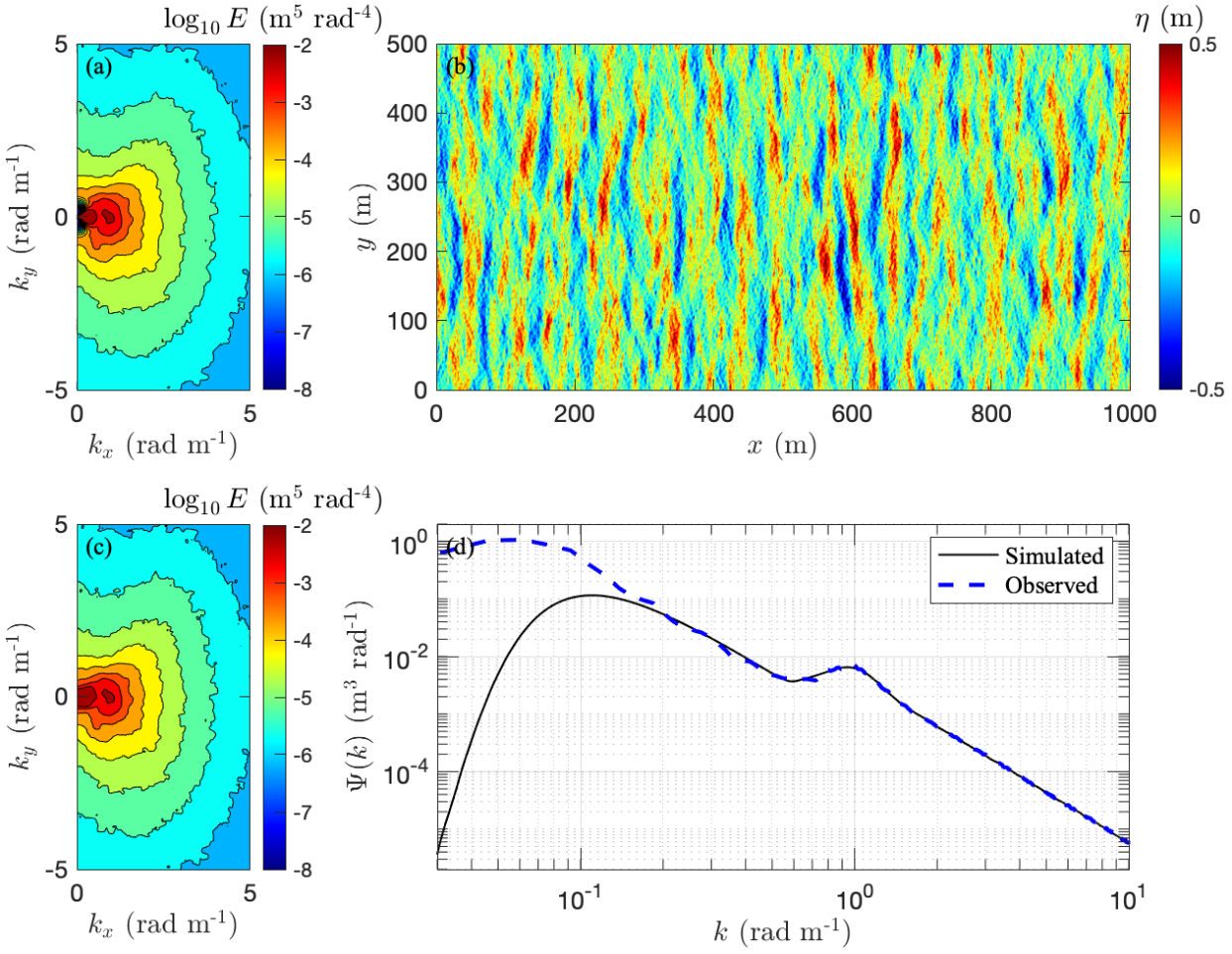

FIG. 1. The initialized random directional wave field. (a) Modeled directional wavenumber spectrum $E(k_x, k_y)$. (b) Initial surface wave elevation $\tilde{\eta}$. (c) Directional wavenumber spectrum measured by Lenain and Pizzo (2021). (d) Comparison of the measured and modeled omnidirectional wave spectra.

where the distance between neighboring peaks is 80 m. The corresponding horizontal gradient is shown in Fig. 2(b) with a magnitude of roughly 0.01 s^{-1}. Following Lenain and Pizzo (2021), the constructed surface current has a peak magnitude of 0.2 m s^{-1} in the direction of and opposing the dominant propagation direction of the surface waves. Moreover, we assume the surface current travels with the internal waves with a phase speed of $c_{sc} = c_{iw} = 0.4$ m s^{-1} in Equation (A13), similar to the value reported in Lenain and Pizzo (2021). After integrating Equation (A14), we obtain the internal wave-induced surface elevation $\bar{\eta}$ with a magnitude of roughly 0.01 m shown in Fig. 2(c). In addition, the corresponding vertical velocity of the surface current is computed with Equation (A16) and shown in Fig. 2(d) with a magnitude of roughly 10^{-3} m s^{-1}.

Accepted for publication in *Journal of Physical Oceanography*. DOI 10.1175/JPO-D-22-0097.1.

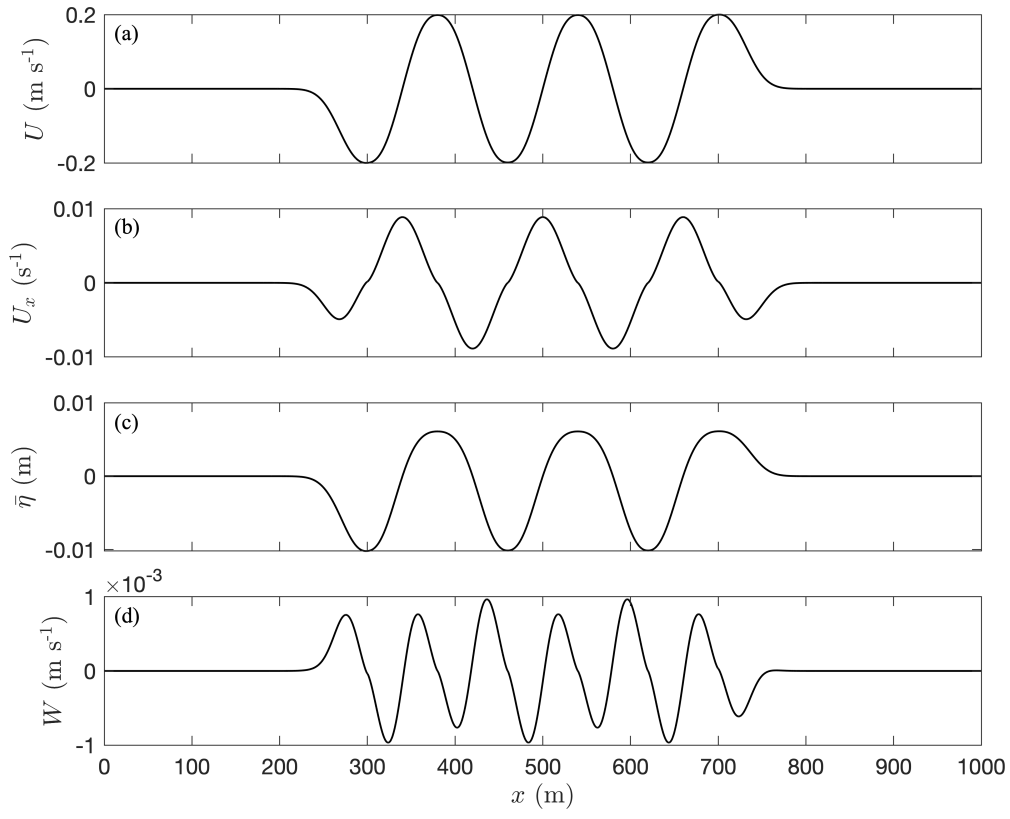

FIG. 2. Modeled internal wave-driven surface current. (a) Horizontal velocity of the surface current and (b) its gradient in the x-direction. (c) Surface elevation induced by the internal waves. (d) Vertical velocity of the surface current.

3) TREATMENT OF WAVE BREAKING

Rather than directly modeling the wave breaking process in a simulation based on the HOS method, a wave smoothing technique is preferred. The most popular was introduced by Xiao et al. (2013), who applied a low-pass filter to remove the energy of waves with short wavelengths and thus model the high-wavenumber dissipation associated with wave breaking. This filter removes the high wavenumber components of the surface elevation and velocity potential in wavenumber space. In addition to the low-pass filter, Tian et al. (2010) proposed a wave breaking model by introducing the concept of an eddy viscosity. When wave breaking occurs in a particular region of the computational domain, two viscous terms based on the second-order horizontal gradients of the surface elevation and velocity potential are added to the model equations to account for energy loss. This treatment of wave breaking is more physical because it is localized and accounts for a single

Accepted for publication in *Journal of Physical Oceanography*. DOI 10.1175/JPO-D-22-0097.1.

wave breaking event. However, its numerical implementation is complicated because it requires calculation of many unknown coefficients, and it only works for one-dimensional problems.

Following Wu (2004), we use a nine-point smoothing technique to model wave breaking events in a two-dimensional problem. In physical space at a given point (x_i, y_j) affected by a wave breaking event, the smoothed wave field is given by

$$\hat{\varphi}\left(x_i, y_j\right) = \frac{1}{9} \sum_{m=i-1}^{i+1} \sum_{n=j-1}^{j+1} \varphi\left(x_m, y_n\right), \tag{11}$$

where φ represents the gravity wave elevation $\tilde{\eta}$ or the velocity potential $\tilde{\phi}$. The area influenced by a wave breaking event is assumed to have a size $l_{b1} \times l_{b2}$, and the center point is given by the location of maximum wave steepness $s = \sqrt{\eta_x^2 + \eta_y^2}$ exceeding a critical value s_b. Equation (11) amounts to a convolution of high-frequency components upon breaking. Similar to the filter proposed by Xiao et al. (2013), the smoothing Equation (11) is also a low-pass filter but is applied to all components in wavenumber space. At the same time, it is applied locally in physical space such that it can model the wave breaking more physically. In the present study, we assume $l_{b1} = l_{b2} = 0.1\lambda_p$ with a critical steepness $s_b = 0.6$ for wave breaking.

4) Numerical configuration

The HOS method is used to simulate the evolution of the surface wave field in deep water modulated by a propagating surface current. The numerical procedure introduced by Dommermuth and Yue (1987) is implemented to solve the model equations that are discretized on a uniform grid in a rectangular domain with periodic boundary conditions. The model equations are then integrated in time using the classical fourth-order Runge–Kutta method with fixed time step size to obtain the evolution of the surface wave field. A third-order series expansion is used to model the modulational instability (Ducrozet et al. 2021). This implies that we take into account the three- and four-wave nonlinear interactions irrespective of whether they are resonant or non-resonant (Tanaka 2001). With the simplified setup presented in this section, we find that the high-order nonlinearity results in a heavy-tailed probability density function of the wave displacements. However, the realistic oceanic conditions measured by Lenain and Pizzo (2021) are less prone to modulational instability implied from the surface wave spectra. We therefore apply a spatially isotropic Gaussian

Accepted for publication in *Journal of Physical Oceanography*. DOI 10.1175/JPO-D-22-0097.1.

smoothing operator with a standard deviation of 1.0 to the wave-current interaction terms defined in Equations (4) and (5) during each time step.

We take the computational domain to have dimensions $L_x = 1000$ m ($L_x \approx 160\lambda_p$) and $L_y = 500$ m ($L_y \approx 80\lambda_p$) in the x- and y-directions, respectively. After considering the aliasing error, the computational domain is discretized with $N_x = 3072$ and $N_y = 1536$ cells in the x- and y-directions, corresponding to approximately $4,700,000$ free wave modes and a spatial resolution of $\Delta x = \Delta y \approx 0.33$ m. We use a time step $\Delta t = T_p/100$, corresponding to a Courant number $C = (\lambda_p/T_p)/(\Delta x/\Delta t) \approx 0.19$. We carry out the simulation for a total time of $T = 60T_p$ and the adjustment scheme of Dommermuth (2000) is applied for natural development of nonlinear self-wave, wave-wave, and wave-current interactions. This is achieved by multiplying the nonlinear terms of the model Equations (2) and (3) by the function

$$R(t) = 1 - \exp\left[-\left(\frac{t}{T_a}\right)^n\right], \tag{12}$$

where the adjustment period $T_a = 20T_p$ and $n = 4$. In our simulation, the initial surface wave field is statistically homogeneous and the surface signature is found to form gradually and is maintained throughout the simulation. After roughly $t = 35T_p$, the simulation reaches a quasi-stationary state after which ensemble averaging is applied to the results discussed in what follows.

3. Results

a. Surface Signature of Internal Waves

The surface signature induced by internal waves is distinct and can often be directly observed from the ocean surface even with the naked eye (Woodson 2018; Lenain and Pizzo 2021). The instantaneous simulated surface elevation at time $t = 45T_p$ is presented in a frame moving with the internal waves in Fig. 3(a). In the range of 200 m $< x <$ 800 m where the internal wave induced surface current is implemented (Fig. 3(c)), changes to the surface elevation are limited to small length scales (corresponding to high wavenumber surface wave components). In contrast, longer waves due to the swell are unchanged (see figure 1 in Lenain and Pizzo (2021)), indicating that the internal waves primarily interact with the wind-generated waves. The wave steepness is illustrated in Fig. 3(b) and is used to quantify the roughness of the ocean surface. Pairs of rough and smooth

Accepted for publication in *Journal of Physical Oceanography*. DOI 10.1175/JPO-D-22-0097.1.

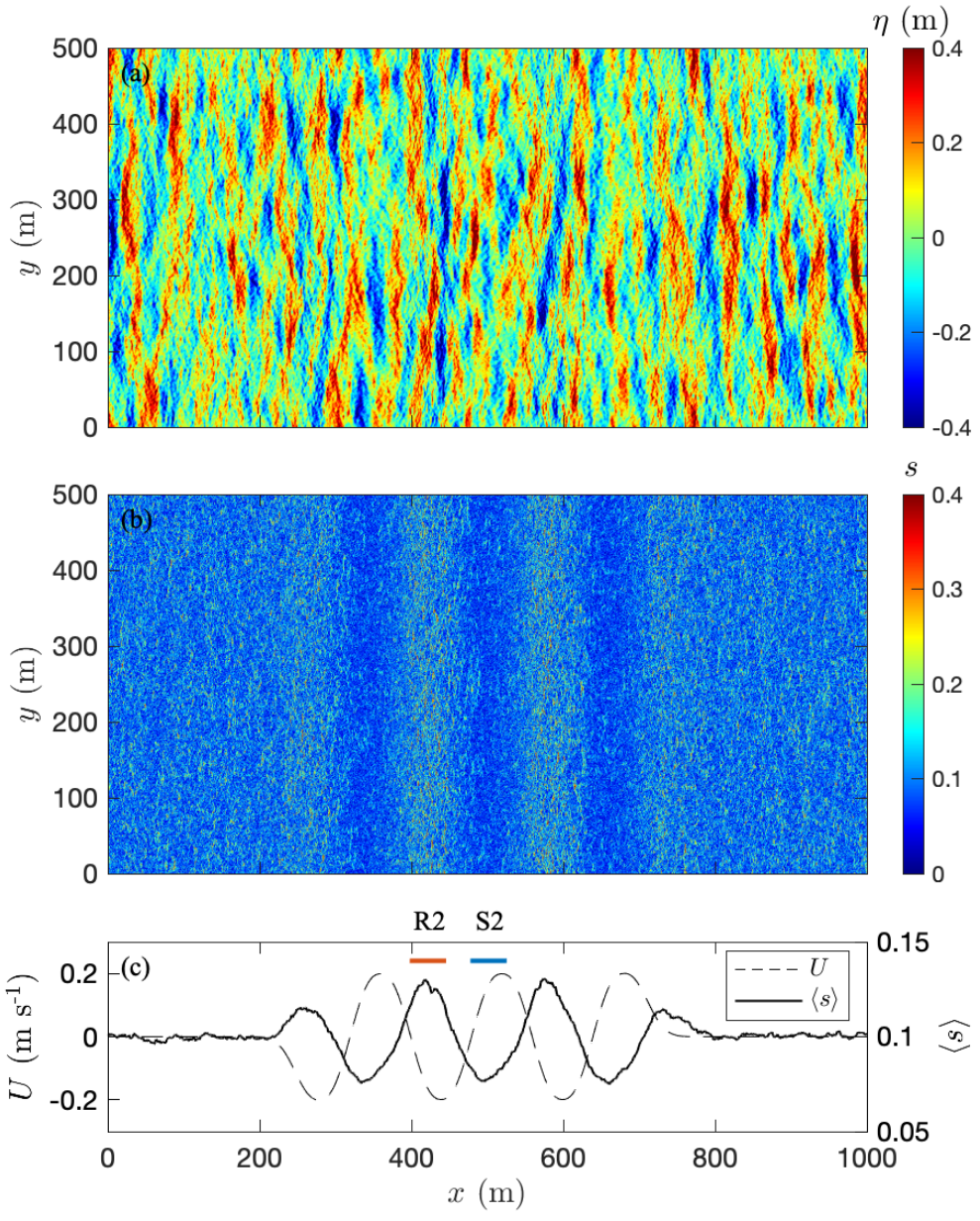

FIG. 3. The surface wave manifestation of an internal wave at time $t = 45T_p$. (a) The surface elevation and (b) the corresponding surface wave steepness. (c) Horizontal velocity of the surface current (solid line) and the time- and laterally-averaged surface slope (dash-dotted line). The areas identified as smooth (S2) and rough (R2) bands are discussed in Section 3b.

regions where the wave steepness is respectively enhanced and reduced are readily observed. These correspond to the pairs of bright and dark bands in satellite images.

Accepted for publication in *Journal of Physical Oceanography*. DOI 10.1175/JPO-D-22-0097.1.

In addition to the x-component velocity of the surface current, the time- and laterally-averaged surface slope $\langle s \rangle$ is plotted in Fig. 3(c). Rough surface bands with increased wave steepness reaching $\langle s \rangle = 0.13$ are formed where there is horizontal convergence of surface currents driven by internal waves ($\partial U/\partial x < 0$). Adjacent to the rough band are smooth regions where the surface current is divergent ($\partial U/\partial x > 0$) and the wave steepness is significantly reduced to $\langle s \rangle = 0.078$ (the background has $\langle s \rangle = 0.1$). This finding is consistent with Woodson (2018), in which a smooth surface occurs on the rising slope of an individual internal wave while a rough surface occurs on its falling slope. In the next section, wave spectra are compared for the smooth (S2) and rough (R2) bands having a width of 48 m, as indicated in Fig. 3(c).

b. Modulation of Surface Wave Spectrum

The surface wave field is significantly modulated by the internal wave-driven surface current according to Lenain and Pizzo (2021). The surface wave spectrogram shown in Fig. 4(b) presents the spatial evolution of the omnidirectional wave spectrum in a frame moving with the internal wave as a function of the along-propagation distance, corresponding to the surface elevation shown in Fig. 3(a). To obtain this figure, the omnidirectional wave spectra are computed in subdomains with a width of 50 m in the x-direction. An overlap of 50% is applied to capture the rapidly evolving spectral properties of the surface waves. The data are then collected in these subdomains and the omnidirectional spectra are computed following Equation (9) with a two-dimensional Hanning window. Fig. 4(b) illustrates the strong spatial modulation of surface conditions by the internal waves, particularly in the high-frequency components for wavenumbers in the range $0.08 - 2.2$ rad m^{-1}. Note that the wind-generated waves in our configuration have a peak wavenumber of roughly $k_p = 1$ rad m^{-1}, and this peak is modulated by the internal waves by as much as 30% across the internal wave bands. Moreover, there is a significant reduction of the spectral magnitude in the smooth bands for shorter waves with $k > 1$ rad m^{-1}. The rapid changes in the surface wave spectrogram at high wavenumbers are consistent with the surface slope signal shown in Fig. 3.

Another feature that can be inferred from Fig. 4 is that the redistribution of energy under the influence of the internal wave packet is fast even though the internal waves are traveling much slower than the surface gravity waves. Surface waves with wavenumbers satisfying $k < 10$ rad m^{-1} have

Accepted for publication in *Journal of Physical Oceanography*. DOI 10.1175/JPO-D-22-0097.1.

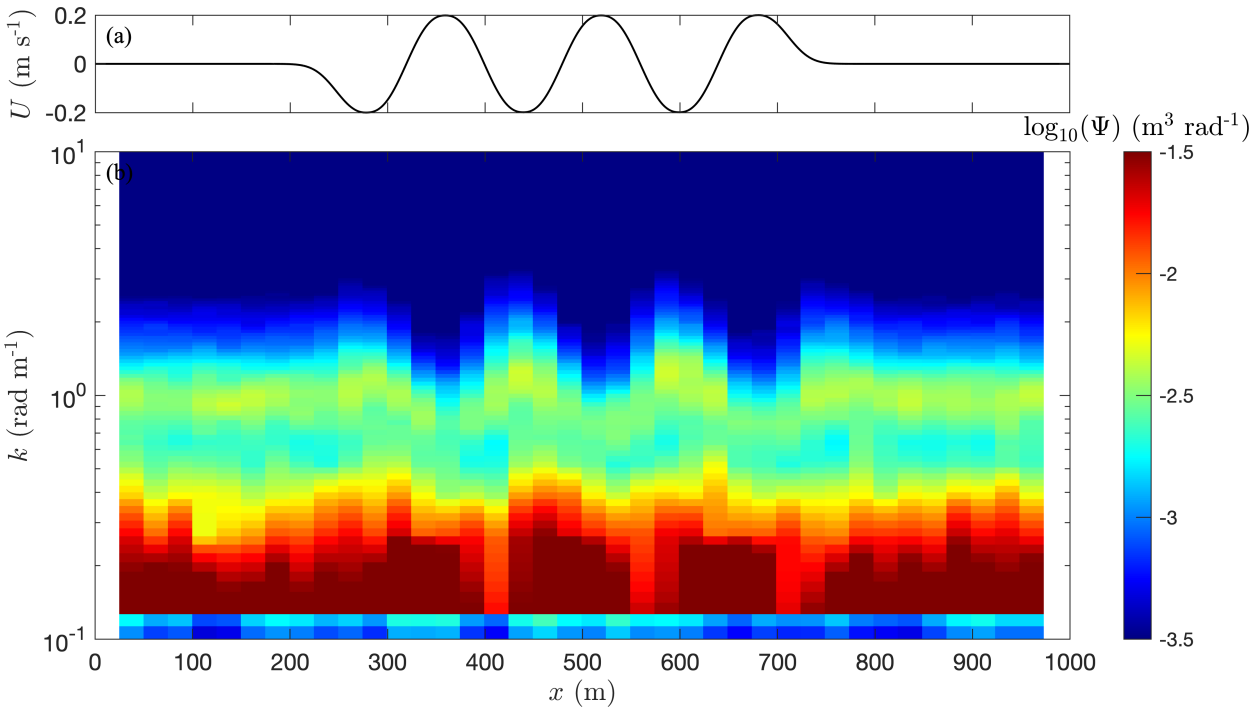

FIG. 4. (a) x-component of the internal wave-driven surface current. (b) The surface wave spectrogram of the wavenumber in the direction of internal wave propagation.

wave phase speeds exceeding 1 m s^{-1}, while the internal wave propagates at just $c_{iw} = 0.4$ m s^{-1}. This strong modulation is highlighted in Fig. 5(a) where the omnidirectional spectra are computed in the smooth and rough bands marked in Fig. 3(c), along with the initial background spectrum for reference. The results indicate a good comparison between the modeled results and the observations for $\Psi > 10^{-3}$ m^3 rad^{-1}. While the energy rapidly decays in the smooth band for wavenumbers in the range $0.08 - 4.0$ rad m^{-1}, an enhancement in the rough band near the peak of the wind waves is observed along with a slight frequency shift of 0.2 rad m^{-1}. This means that the ratio of energy deviation in the rough band is $O(1)$, implying that the surface wave field is strongly modulated by the presence of the internal waves (Lenain and Pizzo 2021), even though weak modulation is often assumed in relaxation theories (Alpers 1985; Rascle et al. 2016). Consequently, our numerical results indicate that the present model based on the HOS method is capable of simulating strong wave-current interactions. However, despite the rather good agreement for $\Psi > 10^{-3}$ m^3 rad^{-1}, the simulated wave energy in both the rough and smooth bands is larger compared to the observations for higher wavenumbers. This is clear in Fig. 5(b) where the results are presented on a logarithmic-

Accepted for publication in *Journal of Physical Oceanography*. DOI 10.1175/JPO-D-22-0097.1.

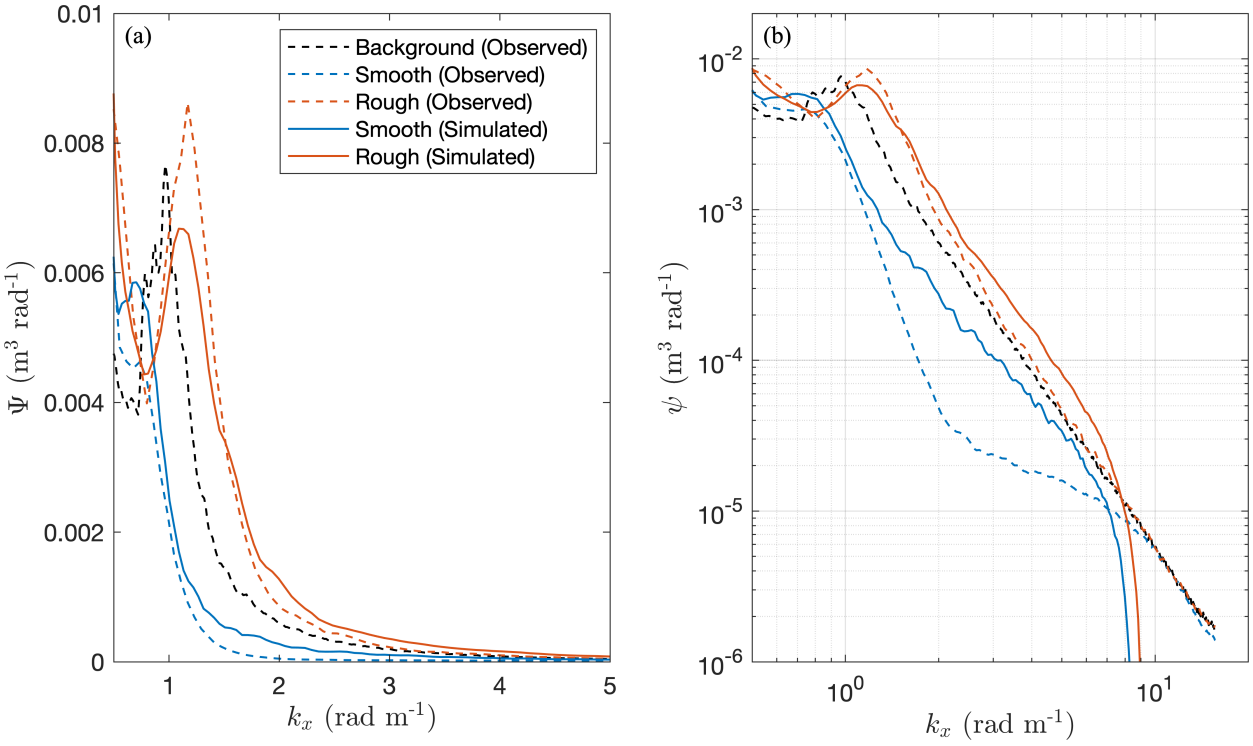

FIG. 5. Simulated and observed (by Lenain and Pizzo (2021)) omnidirectional spectra in the rough and smooth bands indicated in Fig. 3(c) on (a) linear and (b) logarithmic scales.

scale, and may be due to complex processes like near-surface flow re-circulation and mixing not captured by our model based on potential flow theory. Nevertheless, from the perspective of wave energy, this difference is not significant and our model captures the leading-order effects related to the strong wave-current interaction in the smooth and rough bands.

In addition to the energy redistribution shown in Fig. 5, the directional properties of the surface wave spectrum are also rapidly modulated under the influence of the propagating internal wave packet through wave-current interactions. The directional wavenumber spectra $E(k_x, k_y)$ in the rough and smooth bands indicated in Fig. 3(c) are presented in Fig. 6 and compared to the corresponding field observations. The simulated spectrum in the smooth band (Fig. 6(a)) has a rapid increase in angular lobe separation in the $1 - 1.2$ rad m^{-1} range, and then a rapid decay in spectral energy for larger wavenumbers. The field observation in Fig. 6(b) behaves in a similar manner but more significantly such that the wind-wave peak at $k = 1$ rad m^{-1} almost disappears. On the other hand, the simulated spectrum computed in the rough band (Fig. 6(c)) exhibits a distinguishable bimodal distribution with two peaks corresponding to the swell and wind-generated

Accepted for publication in *Journal of Physical Oceanography*. DOI 10.1175/JPO-D-22-0097.1.

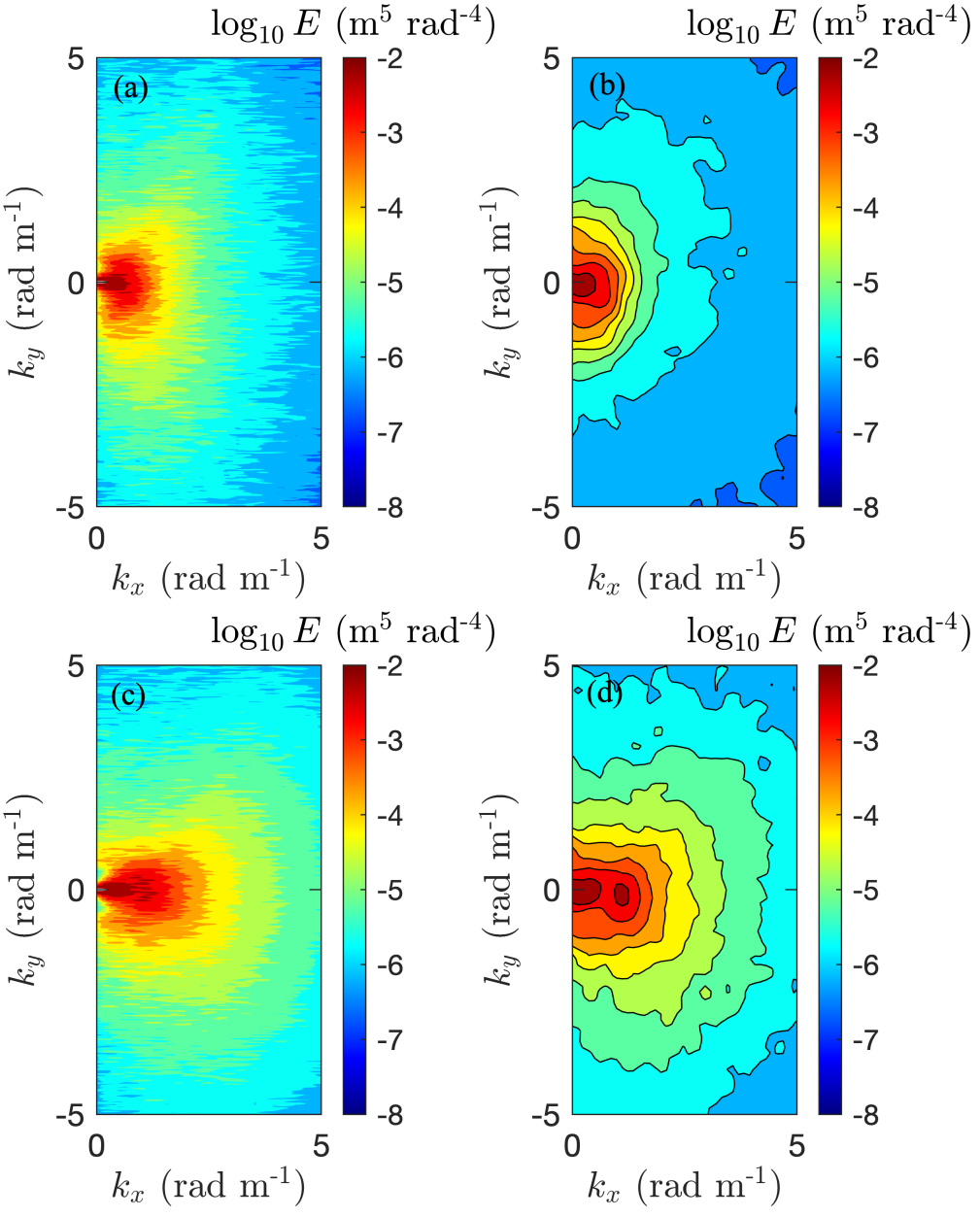

FIG. 6. Directional wavenumber spectra of the surface wave field in the smooth (top row) and rough (bottom row) bands indicated in Fig. 3(c). Simulations are in the left column while observations of Lenain and Pizzo (2021) are in the right column. For clarity, all spectra are zoomed in for wavenumbers less than 5 rad m^{-1}.

waves. This shape is close to the initial spectrum shown in Fig. 1(a) though a clear frequency shift for the wind-generated wave peak and a net decrease in angular separation between energy lobes as a function of wavenumber is clear. The corresponding field observation in Fig. 6(d) has a similar feature compared with the background spectrum in Fig. 1(c). However, as indicated by the

Accepted for publication in *Journal of Physical Oceanography*. DOI 10.1175/JPO-D-22-0097.1.

omnidirectional spectra in Fig. 5, the simulated wave energy at high wavenumbers is enhanced to some degree compared to the observations.

4. Discussion and Conclusions

In this study, we have developed a phase-resolved, wave-current interaction model to simulate the interaction of a random surface wave field with a surface current that varies in both space and time. Using the model, we performed a novel direct simulation to capture the signature of surface roughness induced by a train of internal waves. The model equations are derived based on the variable decomposition and Taylor series expansion following Pan (2020), while the present work considers a propagating, spatially varying surface current moving with the internal waves. The high-order spectral method (Dommermuth and Yue 1987) is used to solve the model equations. The phase-resolved, wave-current interaction model is demonstrated through a simulation with a realistic setting derived from airborne remote sensing observations of Lenain and Pizzo (2021). The surface wave field is initialized with a bimodal spectrum which consists of the measured wind-generated waves and a modeled swell using the Pierson-Moskowitz spectrum. The modeled internal wave-driven surface current has a magnitude of 0.2 m s^{-1} and the wave dynamics of nearly $4,700,000$ independent wave modes are resolved, covering the wide range of length scales manifested by the surface current and short surface waves.

To validate our model with Hao and Shen (2020) where a phase-resolved two-layer fluid model is used, an open-source DJL equation solver is coupled with the present wave-current interaction model for the internal wave-induced surface current. Similar to Hao and Shen (2020), asymmetric behaviour of right- and left-moving surface waves is found in the smooth and rough bands from the wavenumber–frequency slope spectrum, indicating that the present wave-current interaction model is capable of simulating the surface signature of internal waves. After the validation, the present model is applied to simulate the observations of Lenain and Pizzo (2021), where a good comparison of omnidirectional spectra between the modeled results and the observations for $\Psi > 10^{-3}$ m^3 rad^{-1} is obtained. However, the simulated wave energy in both the rough and smooth bands is larger compared to the observations for higher wavenumbers. Several reasons may contribute to this. First, the present model is based on potential flow theory in which complex processes like near-surface flow re-circulation and mixing are not captured which can alter the behavior of surface

Accepted for publication in *Journal of Physical Oceanography*. DOI 10.1175/JPO-D-22-0097.1.

waves. In addition, other factors like bathymetry effects (Chen et al. 2016) or background current shear (Guyenne 2017) are not considered in the present study, which can affect the propagation of internal waves and their surface features. Last, there is an uncertainty in the surface current as it is approximated from observations that do not include the near surface currents and variations of small length scales (Vrećica et al. 2022).

Results from the direct simulation show that the surface manifestation caused by internal waves can be directly observed from the surface elevation and the corresponding surface wave steepness. From the ensemble-averaged surface wave slope, we find that the surface wave field is relatively smooth on the rising slope of an individual internal wave where the surface currents are divergent, and it is relatively rough on the falling slope where they are convergent. The surface wave spectrogram presents the rapid spatial evolution of the omnidirectional wave spectrum in a frame moving with the internal wave as a function of along-propagation distance. These omnidirectional spectra illustrate a rapid redistribution of energy in response to the relatively slowly propagating internal wave. The corresponding directional wavenumber spectra show that the directional properties of the surface wave spectra are also rapidly modulated under the influence of the propagating internal wave packet through strong wave-current interactions. Overall, compared to the observations in Lenain and Pizzo (2021), our numerical results show that the proposed wave-current interaction model is capable of capturing the leading-order effects of the internal wave-driven surface currents on the surface wave spectra.

In summary, we have developed a unique numerical model that allows for the study of the interaction of random surface waves with an arbitrary surface current through the implementation of time-varying wave-current interaction terms in the governing surface wave equations. By imposing a surface current associated with propagating internal waves, the model can be used to study the impact of the surface convergence or divergence due to an arbitrary internal wave on the surface waves. The ability to impose an arbitrary surface current allowed us to simulate the observations of Lenain and Pizzo (2021) in which a train of internal solitary waves modified the surface waves. To our knowledge, this constitutes the first direct simulation in the literature of the modulation of a surface wave spectrum by internal wave-driven surface currents in a real, field-scale setting.

Accepted for publication in *Journal of Physical Oceanography*. DOI 10.1175/JPO-D-22-0097.1.

Acknowledgments. We gratefully acknowledge support of ONR Grants N00014-20-1-2707 and N00014-20-1-2767 (Scientific officers Dr. S. Harper and Dr. L. St. Laurent). We also sincerely thank Dr. L. Lenain and Dr. N. Pizzo for providing us with their open-access data sets (`https://doi.org/10.6075/J0513ZBJ`) needed to generate the figures presented in Lenain and Pizzo (2021).

Data availability statement. All presented data are available at the Stanford Digital Repository (`https://library.stanford.edu/research/stanford-digital-repository`).

APPENDIX A

Derivation of the Model Equations

In this study, we are interested in the surface wave-current interaction in deep water. Based on potential flow theory, the governing equations and the corresponding boundary conditions are given by

$$\nabla^2\phi + \phi_{zz} = 0 \quad \text{in } -\infty < z \le \eta, \tag{A1}$$

$$\eta_t + \nabla\eta\cdot\nabla\phi - \phi_z = 0 \quad \text{at } z = \eta, \tag{A2}$$

$$\phi_t + g\eta + \frac{1}{2}\nabla\phi\cdot\nabla\phi + \frac{1}{2}(\phi_z)^2 = -P_a \quad \text{at } z = \eta, \tag{A3}$$

$$\phi_z = 0 \quad \text{as } z \to -\infty, \tag{A4}$$

where P_a is the pressure at the free surface. Based on the variable decomposition in Equation (1), the total surface elevation η and velocity potential ϕ are decomposed for a surface wave and a surface current component. Thus, the nonlinear kinematic (Equation (A2)) and dynamic (Equation (A3)) boundary conditions can be written in the Zakharov form (Pan 2020) as

$$\tilde{\eta}_t + \nabla\eta\cdot\nabla\tilde{\Phi} - (1+\nabla\eta\cdot\nabla\eta)\,\tilde{\phi}_z + G_k = 0, \tag{A5}$$

$$\tilde{\Phi}_t + g\eta + \frac{1}{2}\left[\nabla\tilde{\Phi}\cdot\nabla\tilde{\Phi} - (1+\nabla\eta\cdot\nabla\eta)\,\tilde{\phi}_z^2\right] + G_d = -P_a, \tag{A6}$$

where the additional terms are given by $G_k = (\bar{\eta}_t + \nabla\eta\cdot\mathbf{U} - W)|_{z=\eta}$ and $G_d = \left[\bar{\phi}_t + \nabla\tilde{\Phi}\cdot\mathbf{U} + (\mathbf{U}\cdot\mathbf{U} + W^2)/2\right]\Big|_{z=\eta}$. These additional terms can be evaluated at $z = \bar{\eta}$ with the

Accepted for publication in *Journal of Physical Oceanography*. DOI 10.1175/JPO-D-22-0097.1.

following relationships

$$\bar{\eta}_t + \nabla\bar{\eta}\cdot\mathbf{U}|_{z=\bar{\eta}} - W|_{z=\bar{\eta}} = 0, \tag{A7}$$

$$\bar{\phi}_t + g\bar{\eta} + \frac{1}{2}\,\mathbf{U}|_{z=\bar{\eta}}\cdot\mathbf{U}|_{z=\bar{\eta}} + \frac{1}{2}\left(W|_{z=\eta}\right)^2 = -P_a, \tag{A8}$$

which are obtained from the kinematic and dynamic boundary conditions when the surface waves are absent. Following Wu (2004) and Pan (2020), we further assume that the vertical gradient of horizontal velocity of the surface current $\mathbf{U}_z$ is small and thus negligible. Consequently, expanding G_k and G_d in Taylor series with respect to the current-induced surface elevation at $z = \bar{\eta}$ gives

$$G_k = \nabla\tilde{\eta}\cdot\mathbf{U}|_{z=\bar{\eta}} - \tilde{\eta}\,W_z|_{z=\bar{\eta}} + O\left((\tilde{\eta})^3\right), \tag{A9}$$

$$G_d = \nabla\tilde{\Phi}\cdot\mathbf{U}|_{z=\bar{\eta}} + \tilde{\eta}\,(W_t + WW_z)|_{z=\bar{\eta}} + \frac{1}{2}\tilde{\eta}^2\left(W_{zt} + W_z^2\right)\Big|_{z=\bar{\eta}} - g\bar{\eta} - P_a + O\left((\tilde{\eta})^3\right), \tag{A10}$$

such that the model Equations (A5) and (A6) can be approximated as

$$\tilde{\eta}_t + \nabla\eta\cdot\nabla\tilde{\Phi} - (1+\nabla\eta\cdot\nabla\eta)\,\tilde{\phi}_z + \nabla\tilde{\eta}\cdot\mathbf{U}|_{z=\bar{\eta}} - \tilde{\eta}\,W_z|_{z=\bar{\eta}} = 0, \tag{A11}$$

$$\begin{aligned}\tilde{\Phi}_t + g\tilde{\eta} + \frac{1}{2}\left[\nabla\tilde{\Phi}\cdot\nabla\tilde{\Phi} - (1+\nabla\eta\cdot\nabla\eta)\,\tilde{\phi}_z^2\right]& \\ + \nabla\tilde{\Phi}\cdot\mathbf{U}|_{z=\bar{\eta}} + \tilde{\eta}\,(W_t + WW_z)|_{z=\bar{\eta}} + \frac{1}{2}\tilde{\eta}^2\left(W_{zt} + W_z^2\right)\Big|_{z=\bar{\eta}} &= 0.\end{aligned} \tag{A12}$$

The model Equations (A11) and (A12) are solved by prescribing a surface current $\mathbf{U}(x, y, z = \bar{\eta}, t)$. In our implementation, we start a simulation with a known surface current at time $t = t_0$. Then, the current travels in the positive x-direction by using

$$\varphi(t) = \mathcal{F}^{-1}\left\{\mathcal{F}\left[\varphi(t = t_0)\right]\exp\left[-ic_{sc}k_x\,(t - t_0)\right]\right\}, \tag{A13}$$

where $\mathcal{F}$ denotes the Fourier transform, φ represents a variable related to the surface current, c_{sc} is the propagation speed of the current, and k_x is the wavenumber in the x-direction.

In order to solve the model Equations (A11) and (A12) with a known surface current $\mathbf{U}(x, y, z = \bar{\eta}, t)$, the information of variables $\bar{\eta}$, W, W_t, and W_{zt} at $z = \bar{\eta}$ are still needed. With $P_a = 0$ and ignoring ∇W (Wu 2004), the current-induced elevation $\bar{\eta}$ can be obtained by applying the horizontal

Accepted for publication in *Journal of Physical Oceanography*. DOI 10.1175/JPO-D-22-0097.1.

gradient to both sides of Equation (A8), giving

$$\nabla\bar{\eta} = -\frac{1}{g}\left(\mathbf{U}_t + \mathbf{U}\cdot\nabla\mathbf{U}\right)\big|_{z=\bar{\eta}}. \tag{A14}$$

Equation (A14) can be numerically integrated for $\bar{\eta}$ by using the Fourier transform with the boundary condition $\bar{\eta}(\infty) = 0$, while $\mathbf{U}_t$ is computed using

$$\varphi_t(t) = \mathcal{F}^{-1}\left\{-ic_{sc}k_x\mathcal{F}\left[\varphi(t)\right]\right\}. \tag{A15}$$

Similarly, $\bar{\eta}_t$ is obtained with a known $\bar{\eta}$. The vertical velocity of the surface current at $z = \bar{\eta}$ is then evaluated using Equation (A7) with

$$W|_{z=\bar{\eta}} = \bar{\eta}_t + \nabla\bar{\eta}\cdot\mathbf{U}|_{z=\bar{\eta}}, \tag{A16}$$

while the corresponding vertical gradient $W_z|_{z=\bar{\eta}} = -\nabla\cdot\mathbf{U}|_{z=\bar{\eta}}$ from the Laplace Equation (A1). Using Equation (A15), we have $W_t|_{z=\bar{\eta}}$ and $W_{zt}|_{z=\bar{\eta}}$ such that our model equations can be solved with the high-order spectral method introduced by Dommermuth and Yue (1987).

We note that, the model equations presented in this section are consistent with those presented by Wu (2004), Wang et al. (2018) and Pan (2020) though the latter works consider the interaction of surface waves with a stationary current and/or different orders of the Taylor series expansions in Equations (A9) and (A10).

APPENDIX B

Model Validation

In order to avoid the singularity encountered in the traditional wave-current interaction theory, Hao and Shen (2020) presents the first-ever effort to directly capture the surface roughness signature induced by ocean internal solitary waves with a deterministic two-layer model for stratified fluids. By capturing over four million wave components, the simulation simultaneously resolves the dynamics of the surface and internal waves. The model successfully captures a surface manifestation characterized by a rough region followed by a smooth region travelling with an internal solitary wave.

Accepted for publication in *Journal of Physical Oceanography*. DOI 10.1175/JPO-D-22-0097.1.

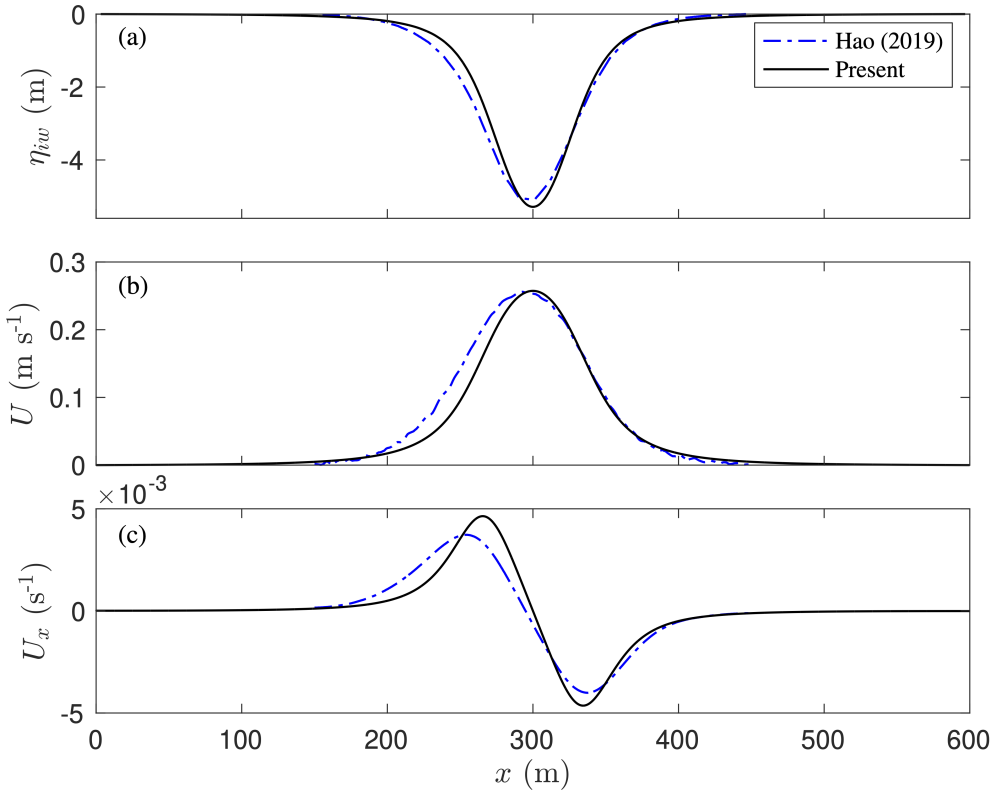

FIG. B1. Comparison of the internal wave and the resulting surface current. (a) Profile of the internal wave denoted by the interface elevation. (b) Profile of the internal wave induced surface current and (c) its horizontal gradient.

To validate the present model, we carry out a simulation in a two-layer setting similar to the setup used by Hao and Shen (2020). The mean depth of the upper layer is $h_u = 7$ m along with a total depth of 147 m. The computational domain has dimensions of $L_x = 600$ m and $L_y = 150$ m in the x- and y-direction, respectively. The corresponding grid numbers are $N_x = 4096$ and $N_y = 1024$ after considering the aliasing error. The directional JONSWAP wave spectrum (Hasselmann et al. 1973) is used to initialize the random surface wave with a wind speed of 7 m s^{-1} at a height of 10 m above the sea surface and a fetch of 9500 m. The directional spreading of wave energy is achieved with the spreading function $D(\theta) = 2/\pi \cos^2\theta$. We use the open-source solver DJLES (Dunphy et al. 2011), a MATLAB/Octave package that finds a mode-one solution to the DJL equation, to obtain the internal wave-driven surface current with a density ratio of 0.997. The computed internal wave has a speed of $c_{iw} = 0.52$ m s^{-1} and its interface elevation is compared to Hao (2019) in the frame moving with the internal wave as shown in Fig. B1(a). The resulting profiles of surface current

Accepted for publication in *Journal of Physical Oceanography*. DOI 10.1175/JPO-D-22-0097.1.

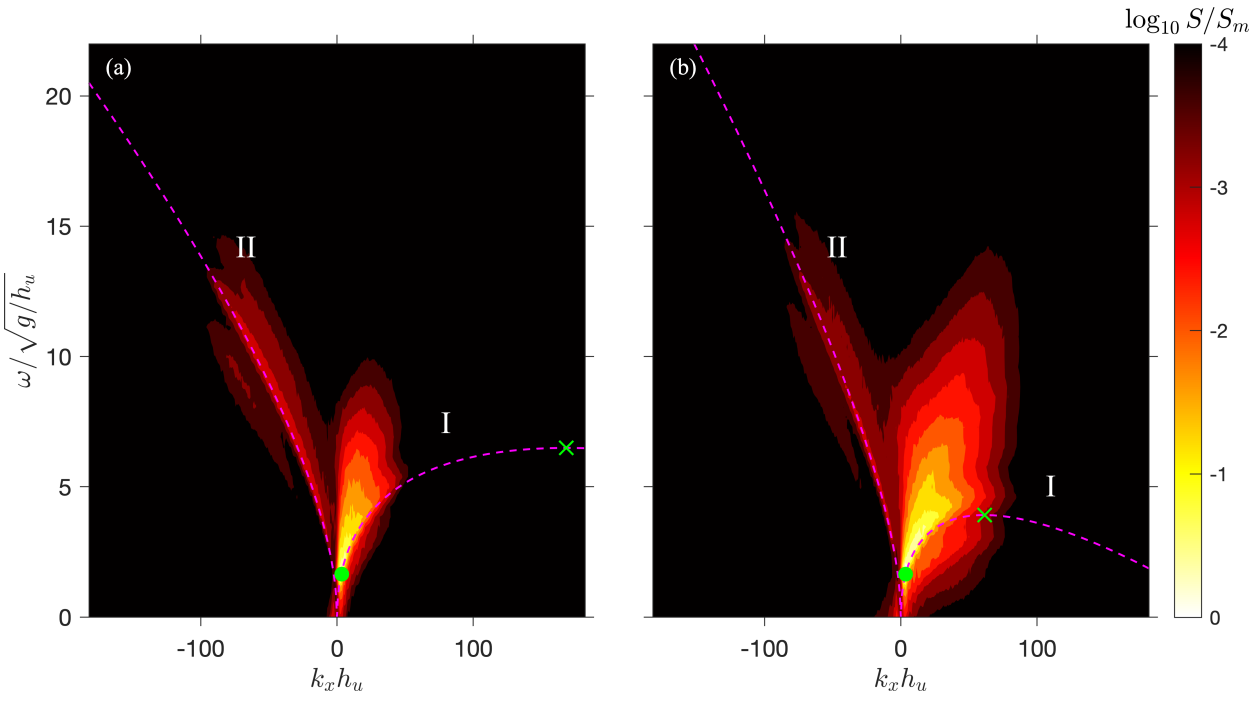

FIG. B2. Wavenumber-frequency slope spectra (normalized by the maximum S_m) of surface waves in the (a) smooth and (b) rough bands. Here, h_u is the mean depth of the upper layer, and the dashed lines denote the dispersion relation of the surface waves in the moving frame of reference. The green filled circle denotes the peak surface wave, while the green crosses denote the maximum frequency of the right-moving surface wave.

and its horizontal gradient are also compared in Fig. B1(b) and (c). From the figure, it is clear that only a small discrepancy can be found in our model setup compared to Hao and Shen (2020).

The surface wave dynamics are analyzed in a frame moving with the internal wave such that the data for the smooth or rough band can be extracted from a fixed subdomain where the averaged slope is correspondingly reduced or enhanced. To better reveal the roughness alternations in the surface wave field, the integrated wavenumber-frequency slope spectrum, defined as $S(k_x,\omega) = \int S(k_x,k_y,\omega)\mathrm{d}k_y$, is calculated for the smooth and rough bands as shown in Fig. B2(a) and (b), respectively. It is clear that both left-moving (region I) and right-moving (region II) surface waves can be found while the right-moving component is evidently enhanced in the rough band indicating a strong manifestation of surface roughness. In addition to the contour plot of slope spectrum in Fig. B2, the dispersion relations of the surface waves in the moving frame of reference $\omega = (U_r - c_{iw})k_x + \sqrt{g|k_x|}$ are also shown. Here, U_r is the surface current at the center of the smooth or rough band. Clearly, we find that the dispersion relations mark the edges of the slope spectra

Accepted for publication in *Journal of Physical Oceanography*. DOI 10.1175/JPO-D-22-0097.1.

with the maximum frequencies of the right-moving surface wave $\omega_m = -g/4(U_r - c_{iw})$ which are denoted by the green crosses. The asymmetric behaviour of right- and left-moving surface waves are found to contribute to the surface signature formation and features are similar to those shown in figure 4 of Hao and Shen (2020).

References

Alpers, W., 1985: Theory of radar imaging of internal waves. *Nature*, **314 (6008)**, 245–247, https://doi.org/10.1038/314245a0.

Bai, X., Z. Liu, X. Li, and J. Hu, 2014: Generation sites of internal solitary waves in the southern Taiwan Strait revealed by MODIS true-colour image observations. *International Journal of Remote Sensing*, **35 (11-12)**, 4086–4098, https://doi.org/10.1080/01431161.2014.916453.

Bakhanov, V. V., and L. A. Ostrovsky, 2002: Action of strong internal solitary waves on surface waves. *J. Geophys. Res. Oceans*, **107 (C10)**, 3139, https://doi.org/10.1029/2001JC001052.

Chen, B.-F., Y.-J. Huang, B. Chen, and S.-Y. Tsai, 2016: Surface wave disturbance during internal wave propagation over various types of sea bottoms. *Ocean Eng.*, **125**, 214–225, https://doi.org/10.1016/j.oceaneng.2016.08.011.

Choi, W., M. Chabane, and T. M. A. Taklo, 2021: Two-dimensional resonant triad interactions in a two-layer system. *J. Fluid Mech.*, **907**, A5, https://doi.org/10.1017/jfm.2020.824.

Craig, W., P. Guyenne, and C. Sulem, 2012: The surface signature of internal waves. *J. Fluid Mech.*, **710**, 277–303, https://doi.org/10.1017/jfm.2012.364.

Dommermuth, D., 2000: The initialization of nonlinear waves using an adjustment scheme. *Wave Motion*, **32 (4)**, 307–317, https://doi.org/10.1016/S0165-2125(00)00047-0.

Dommermuth, D. G., and D. K. P. Yue, 1987: A high-order spectral method for the study of nonlinear gravity waves. *J. Fluid Mech.*, **184**, 267–288, https://doi.org/10.1017/S002211208700288X.

Ducrozet, G., M. Abdolahpour, F. Nelli, and A. Toffoli, 2021: Predicting the occurrence of rogue waves in the presence of opposing currents with a high-order spectral method. *Phys. Rev. Fluids*, **6**, 064 803, https://doi.org/10.1103/PhysRevFluids.6.064803.

Accepted for publication in *Journal of Physical Oceanography*. DOI 10.1175/JPO-D-22-0097.1.

Dunphy, M., C. Subich, and M. Stastna, 2011: Spectral methods for internal waves: indistinguishable density profiles and double-humped solitary waves. *Nonlinear Process. Geophys.*, **18 (3)**, 351–358, https://doi.org/10.5194/npg-18-351-2011.

Goda, Y., 1975: Computation of refraction and diffraction of sea waves with Mitsuyasu's directional spectrum. *Tech. Note of Port and Harbour Res. Inst.*, **230**, 45.

Goda, Y., 1999: A comparative review on the functional forms of directional wave spectrum. *Coast. Eng. J.*, **41 (1)**, 1–20, https://doi.org/10.1142/S0578563499000024.

Guyenne, P., 2017: A high-order spectral method for nonlinear water waves in the presence of a linear shear current. *Comput. Fluids*, **154**, 224–235, https://doi.org/10.1016/j.compfluid.2017.06.004.

Hao, X., 2019: A song of atmosphere and ocean: modeling and simulation-based study of nonlinear waves. Ph.D. thesis, University of Minnesota, 1-141 pp., Minneapolis, MN, USA.

Hao, X., and L. Shen, 2020: Direct simulation of surface roughness signature of internal wave with deterministic energy-conservative model. *J. Fluid Mech.*, **891**, R3, https://doi.org/10.1017/jfm.2020.200.

Hao, X., J. Wu, J. S. Rogers, O. B. Fringer, and L. Shen, 2022: A high-order spectral method for effective simulation of surface waves interacting with an internal wave of large amplitude. *Ocean Modelling*, **173**, 101 996, https://doi.org/10.1016/j.ocemod.2022.101996.

Hasselmann, K. F., and Coauthors, 1973: Measurements of wind-wave growth and swell decay during the Joint North Sea Wave Project (JONSWAP). Tech. rep., Ergänzungsheft zur Deutschen Hydrographischen Zeitschrift, Reihe A.

Helfrich, K. R., and W. K. Melville, 2006: Long nonlinear internal waves. *Annu. Rev. Fluid Mech.*, **38 (1)**, 395–425, https://doi.org/10.1146/annurev.fluid.38.050304.092129.

Hughes, B. A., 1978: The effect of internal waves on surface wind waves 2. Theoretical analysis. *J. Geophys. Res. Oceans*, **83 (C1)**, 455–465, https://doi.org/10.1029/JC083iC01p00455.

Accepted for publication in *Journal of Physical Oceanography*. DOI 10.1175/JPO-D-22-0097.1.

Jiang, S. W., G. Kovačič, D. Zhou, and D. Cai, 2019: Modulation-resonance mechanism for surface waves in a two-layer fluid system. *J. Fluid Mech.*, **875**, 807–841, https://doi.org/10.1017/jfm.2019.501.

Klahn, M., P. A. Madsen, and D. R. Fuhrman, 2020: On the accuracy and applicability of a new implicit taylor method and the high-order spectral method on steady nonlinear waves. *Proc. R. Soc. A: Mathematical, Physical and Engineering Sciences*, **476 (2243)**, 20200 436, https://doi.org/10.1098/rspa.2020.0436.

Lenain, L., and N. Pizzo, 2021: Modulation of surface gravity waves by internal waves. *J. Phys. Oceanogr.*, **51 (9)**, 2735–2748, https://doi.org/10.1175/JPO-D-20-0302.1.

Lewis, J. E., B. M. Lake, and D. R. S. Ko, 1974: On the interaction of internal waves and surface gravity waves. *J. Fluid Mech.*, **63 (4)**, 773–800, https://doi.org/10.1017/S0022112074002199.

Lyzenga, D. R., and J. R. Bennett, 1988: Full-spectrum modeling of synthetic aperture radar internal wave signatures. *J. Geophys. Res. Oceans*, **93 (C10)**, 12 345–12 354, https://doi.org/10.1029/JC093iC10p12345.

Magalhães, J. M., W. Alpers, A. M. Santos-Ferreira, and J. C. da Silva, 2021: Surface wave breaking caused by internal solitary waves: Effects on radar backscattering measured by SAR and radar altimeter. *Oceanography*, https://doi.org/10.5670/oceanog.2021.203.

Magalhães, J. M., and J. C. B. da Silva, 2018: Internal solitary waves in the Andaman Sea: New insights from SAR imagery. *Remote Sens.*, **10 (6)**, https://doi.org/10.3390/rs10060861.

Mitsuyasu, H., F. Tasai, T. Suhara, S. Mizuno, M. Ohkusu, T. Honda, and K. Rikiishi, 1975: Observations of the directional spectrum of ocean waves using a cloverleaf buoy. *J. Phys. Oceanogr.*, **5 (4)**, 750–760, https://doi.org/10.1175/1520-0485(1975)005⟨0750:OOTDSO⟩2.0.CO;2.

Ortiz-Suslow, D. G., and Coauthors, 2019: Interactions between nonlinear internal ocean waves and the atmosphere. *Geophys. Res. Lett.*, **46 (15)**, 9291–9299, https://doi.org/10.1029/2019GL083374.

Pan, Y., 2020: On the model formulations for the interaction of nonlinear waves and current. *Wave Motion*, **96**, 102 587, https://doi.org/10.1016/j.wavemoti.2020.102587.

Accepted for publication in *Journal of Physical Oceanography*. DOI 10.1175/JPO-D-22-0097.1.

Pierson, W. J., and L. Moskowitz, 1964: A proposed spectral form for fully developed wind seas based on the similarity theory of S. A. Kitaigorodskii. *J. Geophys. Res. (1896-1977)*, **69 (24)**, 5181–5190, https://doi.org/10.1029/JZ069i024p05181.

Rascle, N., F. Nouguier, B. Chapron, A. Mouche, and A. Ponte, 2016: Surface roughness changes by finescale current gradients: Properties at multiple azimuth view angles. *J. Phys. Oceanogr.*, **46 (12)**, 3681–3694, https://doi.org/10.1175/JPO-D-15-0141.1.

Romero, L., L. Lenain, and W. K. Melville, 2017: Observations of surface wave–current interaction. *J. Phys. Oceanogr.*, **47 (3)**, 615–632, https://doi.org/10.1175/JPO-D-16-0108.1.

Santos-Ferreira, A. M., and Coauthors, 2022: Effects of surface wave breaking caused by internal solitary waves in SAR altimeter: Sentinel-3 copernicus products and advanced new products. *Remote Sens.*, **14 (3)**, https://doi.org/10.3390/rs14030587.

Smith, J., 1983: On surface gravity waves crossing weak current jets. *J. Fluid Mech.*, **134**, 277–299, https://doi.org/10.1017/S0022112083003365.

Taklo, T. M. A., and W. Choi, 2020: Group resonant interactions between surface and internal gravity waves in a two-layer system. *J. Fluid Mech.*, **892**, A14, https://doi.org/10.1017/jfm.2020.180.

Tanaka, M., 2001: Verification of Hasselmann's energy transfer among surface gravity waves by direct numerical simulations of primitive equations. *J. Fluid Mech.*, **444**, 199–221, https://doi.org/10.1017/S0022112001005389.

Tian, Z., M. Perlin, and W. Choi, 2010: Energy dissipation in two-dimensional unsteady plunging breakers and an eddy viscosity model. *J. Fluid Mech.*, **655**, 217–257, https://doi.org/10.1017/S0022112010000832.

Vrećica, T., N. Pizzo, and L. Lenain, 2022: Airborne observations of shoaling and breaking internal waves. *Geophysical Research Letters*, **49 (21)**, e2022GL100 622, https://doi.org/10.1029/2022GL100622.

Wang, J., Q. Ma, and S. Yan, 2018: A fully nonlinear numerical method for modeling wave-current interactions. *J. Comput. Phys.*, **369**, 173–190, https://doi.org/10.1016/j.jcp.2018.04.057.

Accepted for publication in *Journal of Physical Oceanography*. DOI 10.1175/JPO-D-22-0097.1.

Woodson, C., 2018: The fate and impact of internal waves in nearshore ecosystems. *Annu. Rev. Mar. Sci.*, **10 (1)**, 421–441, https://doi.org/10.1146/annurev-marine-121916-063619.

Wu, G., 2004: Direct simulation and deterministic prediction of large-scale nonlinear ocean wave-field. Ph.D. thesis, Massachusetts Institute of Technology, Cambridge, MA, USA.

Xiao, W., Y. Liu, G. Wu, and D. K. P. Yue, 2013: Rogue wave occurrence and dynamics by direct simulations of nonlinear wave-field evolution. *J. Fluid Mech.*, **720**, 357–392, https://doi.org/10.1017/jfm.2013.37.

Zakharov, V. E., 1968: Stability of periodic waves of finite amplitude on the surface of a deep fluid. *J. Appl. Mech. Tech. Phys.*, **9 (2)**, 190–194, https://doi.org/10.1007/BF00913182.

Accepted for publication in *Journal of Physical Oceanography*. DOI 10.1175/JPO-D-22-0097.1.